Dalton Transactions

ROYAL SOCIETY OF CHEMISTRY

COMMUNICATION

View Article Online
View Journal | View Issue

Check for updates

Cite this: *Dalton Trans.*, 2026, **55**, 1653

Received 26th September 2025,
Accepted 1st January 2026

DOI: 10.1039/d5dt02300a

rsc.li/dalton

Open Access Article. Published on 15 January 2026. Downloaded on 4/19/2026 12:24:00 PM.
This article is licensed under a Creative Commons Attribution 3.0 Unported Licence.

Interzeolite-type transformation between microporous titanosilicates

Stanislav Ferdov [a,b]

This work reveals the first example of an interzeolite-type transformation between microporous heteropolyhedral silicates. In KOH solution, preformed spherulitic particles of the microporous titanosilicate ETS-4 (Engelhard Titanium Silicate-4) transform into single crystals of GTS-1 (Grace Titanium Silicate-1). Mechanistically, the transformation follows a distinct reversed crystallization pathway, beginning on the surface of a seed particle and ending in the reconstructive self-assembly of multiple single crystals. In addition to advancing synthesis methodologies for microporous titanosilicates, this work provides mechanistic insights into a crystallization route that enables templating of the crystal morphology through particle self-assembly.

Crystalline microporous silicates typically develop from a gel growth medium, where two crystallization models are possible: (1) classical crystal growth including a stepwise atom-by-atom attachment process, as described by the nucleation and growth theory,[1,2] and (2) non-classical crystal growth involving particle-based assembly, where amorphous or crystalline nanoparticles merge to form larger crystalline structures.[3] As part of the non-classical model, reversed crystal growth is a sub-model where the crystallization starts from the surface to the center of crystalline[4] or amorphous aggregates.[5] This type of crystallization has been described for zeolites,[4–11] metal–organic frameworks,[12] perovskites,[13] metal oxides[14,15] and hydroxides.[16,17] In the family of zeolites, reversed crystallization generally includes the formation of nanoparticles, their aggregation, surface recrystallization and the formation of single crystals as described for the **ANA** type of zeolite.[4] In other instances, as for the **LTA** zeolite, the recrystallization may occur only on the surface forming a crystalline shell and an amorphous core.[7] Prolongation of the time for crystallization leads to nucleation and growth of clusters of sodalite nanoplates, which starts from the amorphous core and expands to the surface consuming the zeolite A crystals.[6] Similar to zeolites, microporous mixed polyhedral silicates composed of SiO_4 tetrahedra and MO_x (M – transition or other metal ions with coordination higher than four) polyhedra crystallize from gel growth media but their mechanism of crystallization is less explored. **ETS-4** is one of the most studied members of the family of microporous titanosilicates known for its thermal foaming,[18] biomedical,[19] ion exchange,[20] and gas separation properties.[21] **ETS-4** is a stoichiometric metastable phase and in some systems at longer crystallization times transforms into another microporous titanosilicate-**1**,[22] an analogue of the rare mineral ivanyukite.[23] Although interzeolite transformation (IZT), in which a parent phase is transformed into a new framework, has been extensively studied in tetrahedral silicate systems,[24–26] the transformation of pre-formed heteropolyhedral silicates has remained unexplored until now.

This study aims to demonstrate the transformation of **ETS-4** into **GTS-1**, the first example of interstructural transformation in the class of microporous titanosilicates. The specific transformation uncovers a distinct mechanistic process in which pre-existing spherulitic **ETS-4** particles are progressively reconstructed into self-assembled single crystals of the microporous titanosilicate **GTS-1**.

Fig. 1a shows the powder XRD patterns following the transformation of **ETS-4** into **GTS-1**. **ETS-4** was indexed in the orthorhombic space group *Cmmm* with lattice parameters a = 23.2272, b = 7.1751, c = 6.9727 Å[27] using PDF: 96-400-2325, while **GTS-1** was indexed in the cubic space group $P\bar{4}3$ m with lattice parameter a = 7.7647 Å (PDF: 96-153-3728).[28] As the synthesis time increased to 60 and 120 minutes, the intensity of the **ETS-4** diffraction peaks progressively decreased by 20% and 43%, respectively, indicating a gradual loss of crystallinity. By 150 minutes, **ETS-4** was fully transformed into **GTS-1**. The intensity of the powder XRD peaks of **GTS-1** continued to increase with longer synthesis times (1440 and 10080 min), showing improved crystallinity without phase change (Fig. S1). Following its formation, GTS-1 remains structurally stable, although longer reaction times enhance its crystallinity (Fig. S1), reflecting that time governs crystal maturation rather

[a]*Physics Centre of Minho and Porto Universities (CF-UM-UP), University of Minho, 4710-057 Braga, Portugal. E-mail: sferdov@fisica.uminho.pt*
[b]*Laboratory of Physics for Materials and Emergent Technologies, LaPMET, University of Minho, 4710-057 Braga, Portugal*

Open Access Article. Published on 15 January 2026. Downloaded on 4/19/2026 12:24:00 PM.
This article is licensed under a Creative Commons Attribution 3.0 Unported Licence.

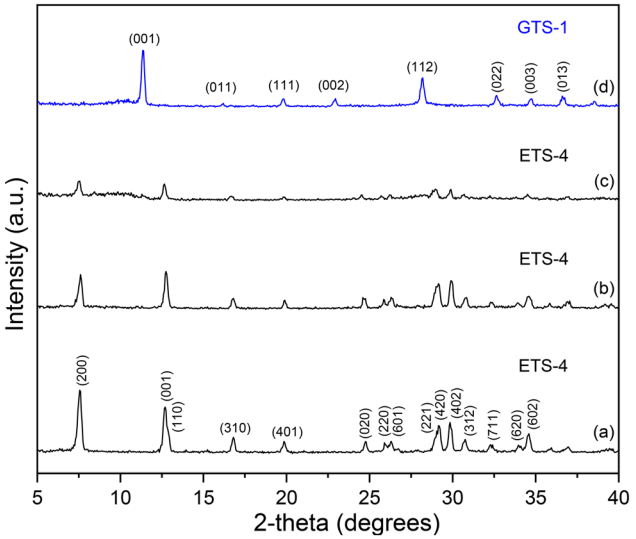

Fig. 1 Indexed powder XRD patterns following the transformation of **ETS-4** into **GTS-1**. (a) The as-synthesized **ETS-4** treated in KOH solution (1.72 M) at 230 °C for (b) 60 min, (c) 120 min and (d) 150 min.

than phase transformation. Additional experiments (Table S1) with varying KOH concentration and temperature revealed a coupled dependence of the transformation on both variables. Higher temperatures (230 °C) enable the transformation at lower KOH concentration (1.72 M), whereas achieving the same transformation at lower temperature (150 °C) requires substantially higher alkalinity (6.88 M). However, below a critical KOH concentration (0.86 M), the transformation does not occur within the selected reaction time (150 min), even at elevated temperature (Fig. S7).

Fig. 2a presents the SEM images of the as-synthesized **ETS-4**, showing particles approximately 40 μm in size. A characteristic radial intergrowth of lamellae-like crystals gives rise to a distinct multilayered, spherulitic morphology, consistent with previous reports on **ETS-4**.[22] After 60 minutes of treatment in KOH solution, sporadic nucleation of layer-like nanoparticles (≈200 nm) (Fig. 2b) with an individual layer thickness of about 20 nm was observed on the **ETS-4** surface (Fig. S2). At this stage, the Si/Ti ratio in both the nanoparticles and the parent crystal surface was 1.1 (Fig. S3), which deviated substantially from the measured value of 2.2 for the as-synthesized **ETS-4**. In the absence of XRD peaks corresponding to any secondary phase, this deviation may indicate surface-initiated amorphization, with both the newly formed particles and the underlying surface showing chemical compositions inconsistent with the original **ETS-4** framework. The observed etched morphology (Fig. S2) is consistent with partial dissolution of the **ETS-4** surface, which could create localized supersaturation of silicate and titanate species near the solid–liquid interface and thereby favor nanoparticle precipitation.[29] After 120 minutes of synthesis, the continued dissolution of **ETS-4** generates a higher concentration of dissolved silica and titania species. This abundance promotes a uniform deposition of layer-like nanoparticles across the entire parent particle (Fig. 2c). Interestingly, the layer thickness of the branched nanoparticles is maintained at approximately 20 nm (Fig. S4). The ongoing dissolution–precipitation cycle is followed by a significant loss of long-range order, as indicated by the substantial decrease in peak intensity of the XRD pattern (Fig. 1c). The spherulitic **ETS-4** particles covered with layer-like nanoparticles exhibit more than a 40% loss in crystallinity compared to the parent **ETS-4** sample, indicating significant structural degradation. Importantly, no well-defined diffraction peaks corresponding to any secondary crystalline phase are observed. Moreover, the Si/Ti ratio (1.8) of the nanoparticles (Fig. S5) deviates markedly from the measured value of 2.2 for

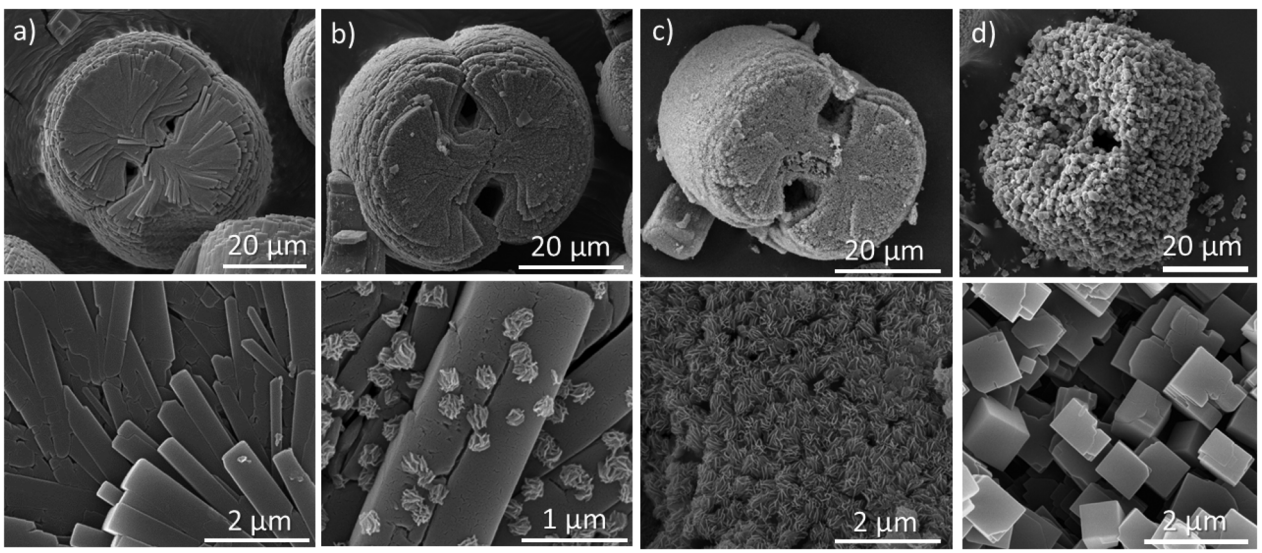

Fig. 2 SEM images showing the evolution of the (a) as-synthesized **ETS-4** particles after (b) 60 min, (c) 120 min and (d) 150 min of hydrothermal treatment in KOH solution.

This journal is © The Royal Society of Chemistry 2026

Open Access Article. Published on 15 January 2026. Downloaded on 4/19/2026 12:24:00 PM.
This article is licensed under a Creative Commons Attribution 3.0 Unported Licence.

ETS-4. This compositional mismatch suggests that the nanoparticles do not belong to the **ETS-4** framework. While a detailed understanding of their structural role lies beyond the scope of this work, future studies could further clarify their involvement in the degradation process. Fig. 2d shows the SEM images of a replica of **ETS-4** composed of self-organized cube-like single crystals of **GTS-1** obtained after 150 minutes of hydrothermal treatment. These submicron crystals (600–900 nm) follow the curvatures of the parent spherulitic particle and are attached by their surfaces, showing the templating effect of the **ETS-4** morphology. The self-organization of **GTS-1** crystals may be driven by a combination of thermodynamic factors – such as the minimization of interfacial energy along the basal pinacoid surfaces – and kinetic constraints related to the localized supply of dissolved species,[30] which together promote nearly oriented attachment and relatively uniform growth across the templating **ETS-4** surface.

Considering previous studies, the appearance of nanoparticles on the surface of the dissolving crystals can be attributed to a local dissolution–reprecipitation process, a mechanism well documented in natural and other solid–fluid systems.[31–34] As the parent crystal dissolves, the interfacial solution becomes locally supersaturated with respect to the new phase, promoting heterogeneous nucleation directly on the crystal surface. To capture the very early stages of nucleation of the layered nanoparticles, a synthesis lasting 30 min was performed. The SEM image (Fig. S8) shows approximately 20 nm thick vertically oriented particles with minimal branching. This observation indicates that the upward growth is faster than lateral growth, but it stops quickly because each burst of local supersaturation produces a new nucleation event rather than thickening the existing sheet (Fig. 2b and S9). As synthesis time increases, the degree of branching becomes progressively more pronounced and assembled on the particle surface as shown in Fig. 2c and S10. This surface evolution reflects the transition from primary nucleation to secondary growth and hierarchical organization.

Fig. 3a provides a direct comparison of the framework characteristics of the parent and daughter phases. As in most zeolites, the transformation proceeds from a lower (**ETS-4:** 14.63 Ti + Si/1000 Å^3) to a higher (**GTS-1:** 14.95 Ti + Si/1000 Å^3) framework density, accompanied by a decrease in the silicon-to-metal ratio as determined by EDS analysis (**ETS-4:** Si/Ti = 2.2 → **GTS-1:** Si/Ti = 0.9; Fig. S6). However, unlike zeolites – where the distribution of the two chemically distinct units (SiO_4 and AlO_4) lacks an ordered pattern and involves only tetrahedral coordination – in the parent **ETS-4** phase the metal atoms (Ti) are five- and six-coordinated, forming a regular arrangement of isolated TiO_5 pyramids and chains of corner-sharing TiO_6 octahedra in addition to 8-rings of SiO_4 tetrahedra. Upon transformation to **GTS-1**, the TiO_5 units disappear, and the chains of TiO_6 octahedra reorganize into clusters of four edge-sharing TiO_6 units and the 8-rings are reduced to single SiO_4 tetrahedra (Fig. 3b).

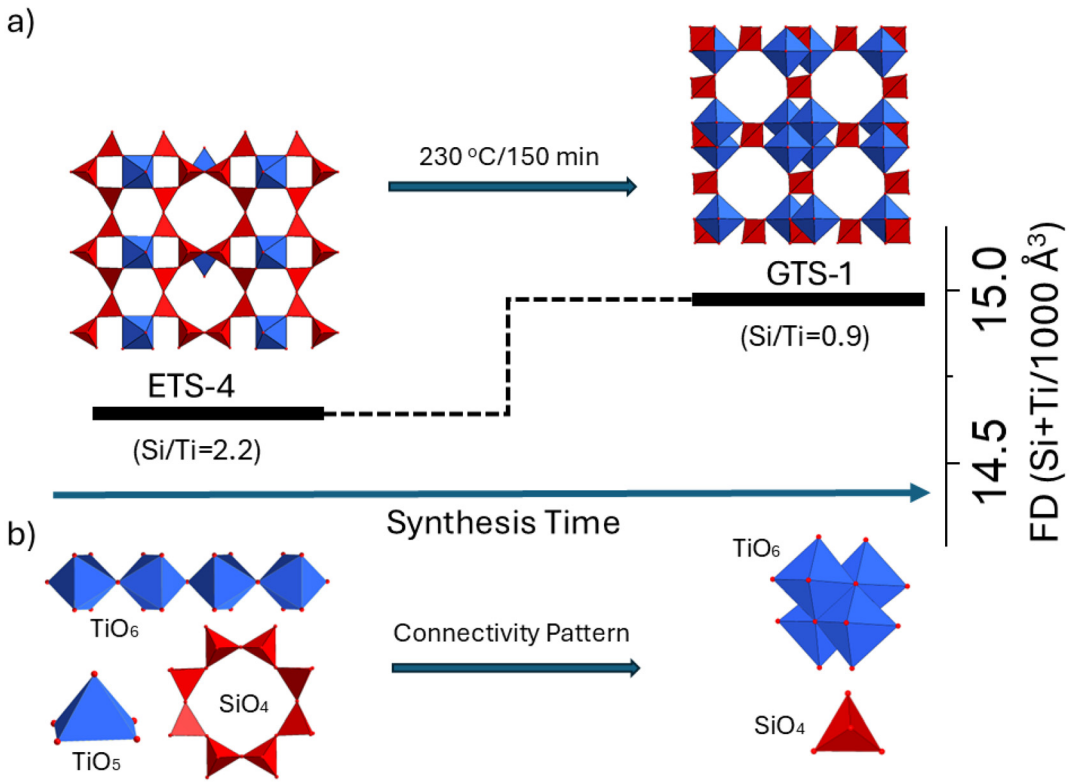

Fig. 3 (a) Transformation from **ETS-4** to **GTS-1** with increasing synthesis time showing framework density (FD) and Si/Ti framework change. (b) Change of connectivity between the building units in the parent and daughter phases.

Open Access Article. Published on 15 January 2026. Downloaded on 4/19/2026 12:24:00 PM.
This article is licensed under a Creative Commons Attribution 3.0 Unported Licence.

Table 1 shows the comparison of the symmetry of the parent (**ETS-4**) and daughter (**GTS-1**) phases with that of zeolites exhibiting a similar tendency upon IZT. The transformations generally progress from lower to higher symmetry (*e.g.*, orthorhombic → cubic, tetragonal → trigonal, orthorhombic → tetragonal, hexagonal → cubic), meaning that the daughter frameworks adopt more symmetric structures than their parents. In synthetic zeolites, however, such low-to-high symmetry transitions appear to be rare, with reported examples including ***BEA → CHA**,[35] **MOR → *BEA**[36] and **AFI → RHO**.[37] Framework rearrangements more typically proceed in the opposite direction, from high to low symmetry, since distortions and local strain tend to break symmetry rather than enhance it. Unlike zeolite systems, where symmetry increases have only been realized through the use of organic structure-directing agents (OSDAs), titanosilicates exhibit such transformations without OSDA assistance, highlighting their intrinsic structural adaptability.

Based on powder XRD data, SEM images, and chemical EDS analyses of samples collected at different synthesis times, Fig. 4 outlines a plausible crystallization pathway for the transformation of **ETS-4** particles into self-assemblies of **GTS-1** single crystals. (1) In the earliest stage, partial dissolution of **ETS-4**, accompanied by sporadic precipitation of chemically distinct layer-like nanoparticles on the parent crystal surface, appears to initiate the structural transformation. At this point, a slight reduction in crystallinity is observed, all XRD reflections remain assignable to **ETS-4**, while the surface chemical composition deviates from the stoichiometric value. (2) In the subsequent stage, the layer-like nanoparticles progressively cover the entire **ETS-4** surface, correlating with a pronounced decrease in overall crystallinity. These nanoparticles lack long-range order and exhibit a significantly lower Si/Ti ratio than the parent **ETS-4** phase. (3) In the final stage, the layer-like nanoparticles reorganize into cube-like single crystals of **GTS-1**.

Compared to previously reported examples of non-classical crystal growth *via* reversed crystallization, the case presented here exhibits two key distinctions: (1) crystallization both initiates in and remains confined to a pre-existing crystalline particle and (2) the nanoparticle building blocks both originate from and reattach to this parent phase. In contrast, other reported systems typically initiate crystallization from an amorphous precursor that evolves to a crystalline phase by the well-known pathways to crystallization by particle/nanocrystal attachment.[3] A mechanism most closely resembling the one presented here is the **FAU**-to-**ANA** transformation, which also begins with a crystalline phase – **FAU** zeolite seeds that aggregate into spheroidal structures – followed by surface-to-interior recrystallization and the formation of faceted **ANA** crystals.[38] These parallels and distinctions underscore the unique advantage of initiating reversed crystallization from an ordered parent phase: it enables greater control over the crystal morphology, allowing preservation or templating of features from the original crystalline source. In this context, starting from crystalline seeds facilitates replication of the external morphology self-assembly of numerous smaller crystals. From the perspective of interzeolite transformation, previous studies have shown that the **FAU** zeolite can be converted to **MFI** *via* a pseudomorphic transformation using **MFI** seeds in NaOH solution.[39] This happens when **FAU** starts to lose its structure, and **MFI** seeds help rebuild it into the **MFI** framework. In another example, hollow spheres of the amorphized **FAU** zeolite were transformed into the **EDI** zeolite.[11] These spheres are composed of amorphous particles that transform over time into the **FAU** structure. Similarly, recrystallization of **FAU** in the presence of surfactants generates mesopores while preserving the external morphology and the overall structure of the parent zeolite.[40,41] The key difference between the **FAU** and **ETS-4** transformations lies in how morphology is preserved. In the **FAU** examples, the transformations occur largely within the original crystal, preserving the external shape while the internal structure reorganizes or recrystallizes. In contrast, the **ETS-4** to **GTS-1** transformation follows a templated, reconstruc-

Table 1 Comparative interstructural transformations between microporous titanosilicates and zeolites leading to a higher symmetry in the daughter phase

Transformation	Symmetry (parent → daughter)	OSDAs	Ref.
ETS-4 → GTS-1	Orthorhombic → cubic	No	This work
***BEA → CHA**	Tetragonal → trigonal	Yes	35
MOR → *BEA	Orthorhombic → tetragonal	Yes	36
AFI → RHO	Hexagonal → cubic	Yes	37

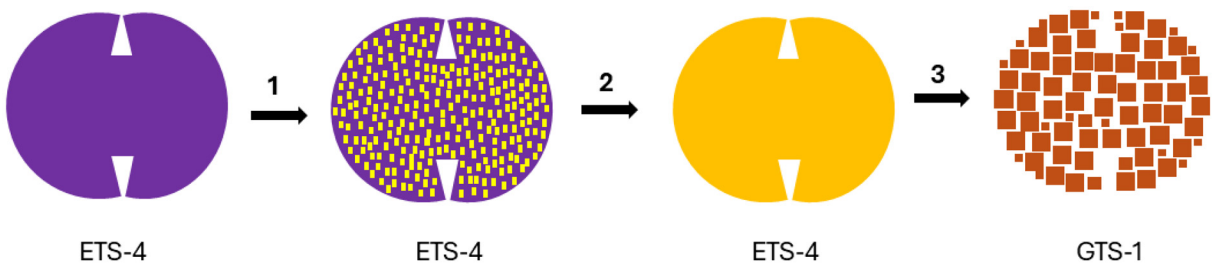

Fig. 4 Schematic presentation of the proposed crystallization pathway leading from **ETS-4** to **GTS-1**. (1) Nucleation and sporadic growth of vertically oriented layer-like nanoparticles on the surface of the parent crystal, exhibiting a chemically distinct composition and no long-range order. (2) Complete coverage of **ETS-4** by these nanoparticles. (3) Transformation into self-assembled single crystals of **GTS-1**.

This journal is © The Royal Society of Chemistry 2026

Open Access Article. Published on 15 January 2026. Downloaded on 4/19/2026 12:24:00 PM. This article is licensed under a Creative Commons Attribution 3.0 Unported Licence.

tive pathway. This process fully replaces the parent structure *via* successive self-assembly of different particles, effectively replicating the original morphology using entirely new building blocks – akin to demolishing a building and reconstructing it with different bricks in the same shape. Such diversity in mechanistic behavior underscores why theoretical and simulation studies have long emphasized that interzeolite transformations cannot be explained by any single structural or energetic descriptor.[42,43] These studies highlight the limitations of using shared building units or framework similarity to predict parent–daughter relationships, and energetic models, while useful, remain incomplete because they depend strongly on composition, solvent effects, and interfacial energetics.[42] Recent molecular simulations further demonstrate that intact parent surfaces, rather than isolated structural fragments, can direct transformation through interface-mediated pathways such as cross-nucleation.[44] Within this broader context, the findings of the present work provide a mechanistic perspective that complements and extends existing theoretical frameworks. Whereas prior models primarily distinguish between dissolution–reprecipitation and diffusionless or topotactic rearrangements, the results highlight a surface-initiated reconstructive pathway that operates through sequential structural reorganization rather than a direct framework rearrangement. This behavior illustrates how interzeolite-type transformations can proceed through intermediate states that couple surface processes with particle-level assembly, revealing a route that is neither conventionally pseudomorphic nor classically topotactic. Such a feature broadens the mechanistic scenarios of interstructural transformations and shows how surface-driven processes can direct the emergence of new microporous architectures.

In conclusion, this study demonstrates that microporous titanosilicates can be obtained through transformation of a preformed microporous phase. **ETS-4** was converted into **GTS-1** *via* a reversed crystallization pathway involving successive pseudomorphic substitutions and structural reorganization. Unlike conventional pseudomorphism, which typically entails internal restructuring, this process is characterized by the nucleation of chemically distinct nanoparticles on the surface of **ETS-4** crystals, followed by their transformation into single crystals of **GTS-1** while preserving the external morphology. This mechanism demonstrates that a pre-existing crystal can serve as an effective template for crystal engineering through self-assembly, offering a rational route for designing titanosilicate microstructures *via* controlled interstructural transformation.

Conflicts of interest

There are no conflicts to declare.

Data availability

The data supporting this article have been included as part of the supplementary information (SI). The supplementary information provides details on the synthesis conditions of the parent phase, the parameters used for the interstructural transformation, and characterization data, including XRD patterns, SEM micrographs, and EDS analyses. See DOI: https://doi.org/10.1039/d5dt02300a.

Acknowledgements

This work was supported by the Portuguese Foundation for Science and Technology (FCT) in the framework of the Strategic Funding UID/04650/2025 (https://doi.org/10.54499/UID/04650/2025) and the SEMAT (University of Minho).

References

1 J. D. H. Donnay and D. Harker, *Am. Mineral.*, 1937, **22**, 446–467.
2 P. Hartman and W. Perdok, *Acta Crystallogr.*, 1955, **8**, 49–52.
3 J. J. De Yoreo, P. U. P. A. Gilbert, N. A. J. M. Sommerdijk, R. L. Penn, S. Whitelam, D. Joester, H. Zhang, J. D. Rimer, A. Navrotsky, J. F. Banfield, A. F. Wallace, F. M. Michel, F. C. Meldrum, H. Cölfen and P. M. Dove, *Science*, 2015, **349**, aaa6760.
4 X. Chen, M. Qiao, S. Xie, K. Fan, W. Zhou and H. He, *J. Am. Chem. Soc.*, 2007, **129**, 13305–13312.
5 Q. Yue, K. Kutukova, A. Li, J. Čejka, E. Zschech and M. Opanasenko, *Chem. – Eur. J.*, 2022, **28**, e202201468.
6 H. Greer, P. S. Wheatley, S. E. Ashbrook, R. E. Morris and W. Zhou, *J. Am. Chem. Soc.*, 2009, **131**, 17986–17992.
7 J. Yao, D. Li, X. Zhang, C.-H. Kong, W. Yue, W. Zhou and H. Wang, *Angew. Chem., Int. Ed.*, 2008, **47**, 8397–8399.
8 Q. Wang, G. Chen and S. Xu, *Microporous Mesoporous Mater.*, 2009, **119**, 315–321.
9 L. Han, J. Yao, D. Li, J. Ho, X. Zhang, C.-H. Kong, Z.-M. Zong, X.-Y. Wei and H. Wang, *J. Mater. Chem.*, 2008, **18**, 3337–3341.
10 S. Ferdov, *Microporous Mesoporous Mater.*, 2020, **303**, 110263.
11 S. Ferdov, *Molecules*, 2024, **29**, 1744.
12 C. Zheng, H. F. Greer, C.-Y. Chiang and W. Zhou, *CrystEngComm*, 2014, **16**, 1064–1070.
13 X. Yang, J. Fu, C. Jin, J. Chen, C. Liang, M. Wu and W. Zhou, *J. Am. Chem. Soc.*, 2010, **132**, 14279–14287.
14 K. Self, H. Zhou, H. F. Greer, Z. R. Tian and W. Zhou, *Chem. Commun.*, 2013, **49**, 5411–5413.
15 B. Zhang, S. Cao, M. Du, X. Ye, Y. Wang and J. Ye, *Catalysts*, 2019, **9**, 91.
16 L.-Y. Chen and Z.-D. Zhang, *J. Phys. Chem. C*, 2008, **112**, 18798–18803.
17 M. T. Buscaglia, V. Buscaglia, C. Bottino, M. Viviani, R. Fournier, M. Sennour, S. Presto, R. Marazza and P. Nanni, *Cryst. Growth Des.*, 2008, **8**, 3847–3855.
18 S. Ferdov, *Angew. Chem., Int. Ed.*, 2013, **52**, 12135–12138.
19 S. Ferdov, E. Shikova, Z. Ivanova, L. T. Dimowa, R. P. Nikolova, Z. Lin and B. L. Shivachev, *RSC Adv.*, 2013, **3**, 8843–8848.

Open Access Article. Published on 15 January 2026. Downloaded on 4/19/2026 12:24:00 PM.
This article is licensed under a Creative Commons Attribution 3.0 Unported Licence.

20 R. P. Nikolova, B. L. Shivachev and S. Ferdov, *Microporous Mesoporous Mater.*, 2013, **165**, 121–126.
21 S. M. Kuznicki, V. A. Bell, S. Nair, H. W. Hillhouse, R. M. Jacubinas, C. M. Braunbarth, B. H. Toby and M. Tsapatsis, *Nature*, 2001, **412**, 720–724.
22 V. Kostov-Kytin, S. Ferdov, Y. Kalvachev, B. Mihailova and O. Petrov, *Microporous Mesoporous Mater.*, 2007, **105**, 232–238.
23 V. N. Yakovenchuk, A. P. Nikolaev, E. A. Selivanova, Y. A. Pakhomovsky, J. A. Korchak, D. y. V. Spiridonova, O. A. Zalkind and S. V. Krivovichev, *Am. Mineral.*, 2009, **94**, 1450–1458.
24 S. Ferdov and R. Gonçalves, *Dalton Trans.*, 2025, **54**, 7621–7626.
25 Z. Liu, A. Chokkalingam, S. Miyagi, M. Yoshioka, T. Ishikawa, H. Yamada, K. Ohara, N. Tsunoji, Y. Naraki, T. Sano, T. Okubo and T. Wakihara, *Phys. Chem. Chem. Phys.*, 2022, **24**, 4136–4146.
26 L. Van Tendeloo, E. Gobechiya, E. Breynaert, J. A. Martens and C. E. A. Kirschhock, *Chem. Commun.*, 2013, **49**, 11737–11739.
27 S. Nair, H.-K. Jeong, A. Chandrasekaran, C. M. Braunbarth, M. Tsapatsis and S. M. Kuznicki, *Chem. Mater.*, 2001, **13**, 4247–4254.
28 A. Tripathi, D. G. Medvedev, J. Delgado and A. Clearfield, *J. Solid State Chem.*, 2004, **177**, 2903–2915.
29 J. J. De Yoreo, E. Nakouzi, B. Jin, J. Chun and C. J. Mundy, *Faraday Discuss.*, 2022, **235**, 9–35.
30 X. Xue, R. L. Penn, E. R. Leite, F. Huang and Z. Lin, *CrystEngComm*, 2014, **16**, 1419–1429.
31 E. Ruiz-Agudo, C. V. Putnis and A. Putnis, *Chem. Geol.*, 2014, **383**, 132–146.
32 A. Putnis and C. V. Putnis, *J. Solid State Chem.*, 2007, **180**, 1783–1786.
33 A. Putnis, *Rev. Mineral. Geochem.*, 2009, **70**, 87–124.
34 R. L. Hartman and H. S. Fogler, *Langmuir*, 2007, **23**, 5477–5484.
35 H. Wu, Y. Lv, J. Zhang, Y. Han and C. Guo, *Microporous Mesoporous Mater.*, 2021, **328**, 111469.
36 B. Wang, L. Ren, J. Zhang, R. Peng, S. Jin, Y. Guan, H. Xu and P. Wu, *Microporous Mesoporous Mater.*, 2021, **314**, 110894.
37 P. Tian, X. Su, Y. Wang, Q. Xia, Y. Zhang, D. Fan, S. Meng and Z. Liu, *Chem. Mater.*, 2011, **23**, 1406–1413.
38 Y. Wang, X. Li, Z. Xue, L. Dai, S. Xie and Q. Li, *J. Phys. Chem. B*, 2010, **114**, 5747–5754.
39 S. Goel, S. I. Zones and E. Iglesia, *Chem. Mater.*, 2015, **27**, 2056–2066.
40 R. Chal, T. Cacciaguerra, S. van Donk and C. Gérardin, *Chem. Commun.*, 2010, **46**, 7840–7842.
41 J. Garcia-Martinez, C. Xiao, K. A. Cychosz, K. Li, W. Wan, X. Zou and M. Thommes, *ChemCatChem*, 2014, **6**, 3110–3115.
42 R. Jain, A. J. Mallette and J. D. Rimer, *J. Am. Chem. Soc.*, 2021, **143**, 21446–21460.
43 A. Navrotsky, O. Trofymluk and A. A. Levchenko, *Chem. Rev.*, 2009, **109**, 3885–3902.
44 C. Chu-Jon, E. Martinez, A. A. Bertolazzo, S. Banik, J. D. Rimer, S. K. R. S. Sankaranarayanan and V. Molinero, *J. Am. Chem. Soc.*, 2024, **146**, 33204–33213.

This journal is © The Royal Society of Chemistry 2026